Japanese Journal of Applied Physics
Vol. 44, No. 9, 2005, pp. L 288–L 291

1-kHz Real-Time Imaging Using a Half-Cycle Terahertz Electromagnetic Pulse

Rakchanok RUNGSAWANG*, Aya MOCHIDUKI, Shin-ichi OOKUMA and Toshiaki HATTORI

Institute of Applied Physics, University of Tsukuba, 1-1-1 Tennodai, Tsukuba 305-8573, Japan

(Received November 8, 2004; accepted December 27, 2004; published February 10, 2005)

Real-time high-speed terahertz (THz) two-dimensional imaging at a frame rate as high as 1 kHz was performed using intense half-cycle THz electromagnetic pulses. The THz source was a 3-cm-gap photoconductive antenna. The distribution of THz electric field was detected by a single optical probe pulse using a high-speed charge–coupled device camera by adopting a phase-sensitive electrooptic detection method. Using the system, we demonstrated imaging of a moving metal object by observing the transmitted beam. The time delay of optical pulses was fixed to probe the THz pulse at the time when the axial THz waveform has the steepest transient, which yields a good image quality. This research opens the window of high-speed imaging in the THz frequency regime. [DOI: 10.1143/JJAP.44.L288]

KEYWORDS: half-cycle electromagnetic pulse, large-aperture photoconductive antenna, terahertz imaging, single-shot imaging, phase-sensitive electrooptic detection

Recent advances in the generation, detection, and manipulation of electromagnetic waves in the terahertz (THz) region, or in the frequency range from 100 GHz to 10 THz, are rapidly increasing their use in spectroscopy and imaging. THz waves can determine various properties of materials, such as semiconductors, dielectrics, proteins, and liquids, in a low-frequency range.[1–3] In addition, the use of THz waves is much safer than that of X-ray since the long-wavelength waves do not ionize or harm the object of interest, particularly biological matter. Consequently, THz waves have been used for non-invasive monitoring of biological tissues.[4] One of the outstanding applications in this field is two-dimensional THz imaging. It was first demonstrated by Wu *et al.*[5] They obtained a two-dimensional intensity distribution of a focused THz beam using an electrooptic (EO) sampling technique and a thermoelectrically cooled charge-coupled device (CCD) camera at frame rates of 38 frames per second (fps), which is comparable to that of a standard television (30 fps). The electric field detection technique and a capturing rate up to 69 fps were used to perform spatio temporal detection of few-cycle THz pulses by Jiang and Zhang.[6] THz images of stationary and moving samples were observed at frame rates of 30 fps and 10 fps, respectively.[7]

Obviously, the accumulation of a larger number of THz pulses per frame and a lower frame rate provide higher image quality. However, increasing the frame rate is one of the imaging challenges because it allows the monitoring of single-time events occurring at a high speed. With a long history of optical imaging, high-speed detection has been successfully and widely applied to basic research and everyday occurrences, such as examining the splash of a water drop at 1000 fps or higher. Because imaging in this mode based on THz waves might open new visual opportunities of high-speed phenomena such as explosions and laser ablations, it is meaningful to achieve THz imaging at a high frame rate, which is comparable to the optical one. However, data acquisition is not limited only by the speed of the image detector, but also by the intensity of the THz radiation, detection technique, and timing. Recently, Miyamaru *et al.* reported a high-frame-rate measurement of a THz beam profile at 1000 fps using a complementary metal oxide semiconductor (CMOS) camera.[8] However, in their report, half of the image data were used as the reference for a subtraction detection mode yielding a high signal-to-noise ratio, with a sample that was not imaged at a high frame rate.

In this letter, we report that we have succeeded in implementing real-time high-speed movies in the THz frequency region at a rate of 1000 fps using a high-speed CCD camera and an intense THz source. A single image was acquired for each THz pulse at a repetition rate of 1 kHz. Using phase-sensitive detection, the THz field was converted to optical intensity using an EO crystal for recording by a CCD camera. The THz field was then calculated and Gaussian filtering was employed to reduce noise. A movie of a moving object was obtained using a single THz pulse per frame.

The schematic of the experimental setup is shown in Fig. 1. A large-aperture photoconductive antenna was used as the THz source. The THz field on the EO crystal modulates the phase of the linearly polarized probe light via the EO effect. The laser system, the bias-voltage generator, and the high-speed CCD camera (Photron, FASTCAM-PCI 2K) were synchronized to a 1 kHz external clock. The exposure time of the CCD camera was set to be 0.5 ms so that the CCD camera could capture the intensity profile of each modulated probe pulse. The emitter was made of a

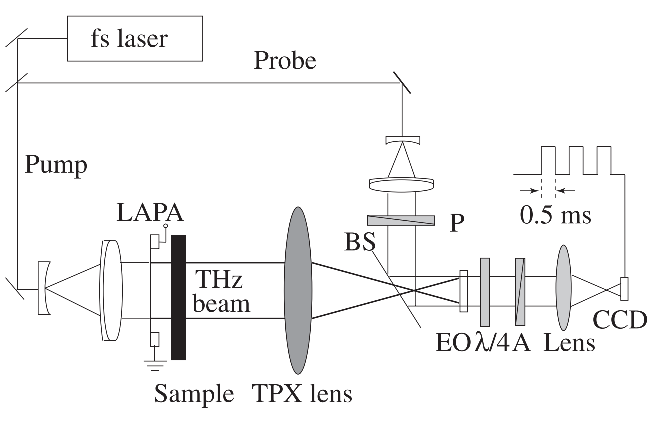

Fig. 1. Schematic of experimental setup. LAPA: large-aperture photoconductive antenna, BS: pellicle beam splitter, EO: electrooptic crystal (ZnTe), $\lambda/4$: quarter-wave plate, P: polarizer, and A: polarization analyzer. The exposure time of the CCD camera is 0.5 ms.

*E-mail address: nok@laserlab.bk.tsukuba.ac.jp

350 μm semi-insulating GaAs wafer. It was pumped using regeneratively amplified femtosecond Ti:sapphire laser pulses, whose pulse width, center wavelength and repetition rate were 150 fs, 800 nm, and 1 kHz, respectively. The pump laser beam was spatially expanded and collimated using a beam expander, and illuminated the area of the 30 mm gap between the electrodes attached to the wafer. Generated THz radiation was focused using a TPX (polymethylpentene; Mitsui Chemicals, Inc.) lens, with the focal length $f = 98.3$ mm, onto a 1-mm thick, $\langle 110 \rangle$-cut ZnTe crystal. The probe beam was made collinear with the THz beam using a pellicle beam splitter. The polarizations of the probe beam and the THz beam were aligned along the $(1\bar{1}0)$ axis of the crystal, i.e., the horizontal direction in the laboratory frame. The probe beam diameter on the crystal was approximately 20 mm, and covered an area of $18 \times 20\,\mathrm{mm}^2$. The ZnTe crystal was placed at a distance of $3/2f$ from the lens, and a quarter-wave plate was placed between the crystal and the analyzer for electric field detection by a phase-sensitive EO sampling method.[9–12)]

The procedures of the THz field detection by the phase-sensitive EO sampling method are as follows. The EO crystal and the quarter-wave plate were inserted between the crossed polarizers. The fast axis of the quarter-wave plate was adjusted to be parallel to the axis of the polarizer. The axis of the analyzer was then rotated by a small angle δ from the old position to induce an optical local oscillator field, which is a phase-shifted fraction of the probe light. The phase retardation of the probe light, θ, due to the EO effect, which is proportional to the THz electric field, can be expressed as[10–12)]

$$\theta = -\delta + \sqrt{\delta^2 + \frac{I - I_b}{I_0}}, \tag{1}$$

when $|\delta|, |\theta| \ll 1$. Here, I_0 is the incident probe light intensity, I_b is the background intensity of the probe light transmitted through the δ-rotated analyzer, and I is the intensity of the transmitted probe light in the presence of the THz field. I_b is not only contributed by optical-bias light from the rotation of the analyzer axis with the angle δ but also by the intrinsic birefringence and light scattering in the EO crystal. In our experiment, the orientation angle of the analyzer was set at $\delta = 0.02$ radian, where probe intensity modulation due to the EO effect was almost optimized.[11)] Using this method, we could achieve a measurement that is sufficiently sensitive to enable imaging by a single THz pulse. The probe pulses, after passing through the analyzer, were collimated by an optical lens and sent to the monochrome high-speed video camera. The image size at the position of the CCD chip was reduced to 1/5 time of that at the ZnTe crystal. The CCD camera can capture images of 256×120 pixels with an 8 bit gray scale at a rate of 1000 fps. The captured image data were stored in the on-board memory, and then transferred to a PC for display and storage.

A large-aperture photoconductive antenna enables a large beam size and a high electric field when biased with a high dc voltage. When a GaAs wafer is used as a photoconductor, it gives almost half-cycle electric pulses.[13,14)] This makes their spectra have a peak near dc. Figure 2 depicts the generated waveform (dashed line) measured at the focus of the TPX lens, $z = 0$, by an EO sampling method. The inset shows its Fourier amplitude (dashed line). As can be seen from the graph, the spatial resolution of the imaging using this THz pulse, determined by one-half of the central wavelength, is limited at about 1 mm. The axial waveform on the image plane of the imaging configuration, at $z = 49.2$ mm, was measured by the same method, as shown in the same figure (solid line). Apparently, it deviates from that measured at the focal plane in which it has a long rise and a fast decay. This is the result of large diffraction in high-frequency components, as can be seen in the inset of Fig. 2. Images of a sample object could be ascertained at the time when the temporal change rate in the THz field was high, namely, 0.2–0.8 ps in the graph because of the dominance of high-frequency components in this time region.[12)] The field distribution on the object plane was imaged onto the EO crystal. The probe pulses mapped the feature on the crystal to the CCD camera according to the phase modulation induced by the THz field. The spatial intensity distribution of the modulated pulses, I, was obtained by the CCD camera. The THz electric field was then calculated by substituting the probe intensity I_0, optical background intensity I_b, and I into eq. (1).

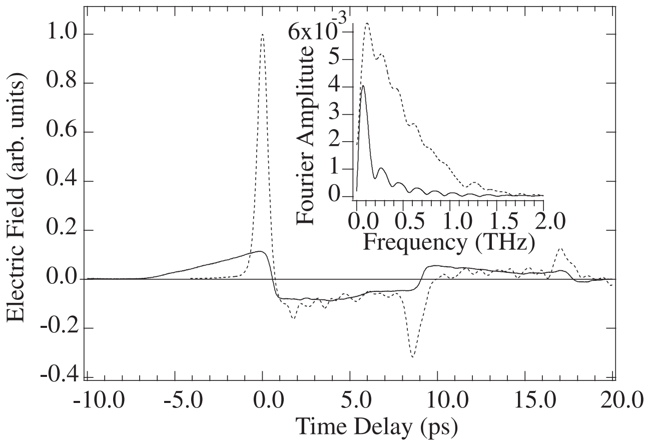

Fig. 2. Normalized THz waveforms measured at focus point $z = 0$ (dashed line) and $z = 49.2$ mm (solid line) using EO sampling detection. The second and third peaks are the reflections of the main THz pulse inside the GaAs wafer and inside the EO crystal, respectively. The inset shows their Fourier amplitudes.

We captured images of a moving object at a frame rate as high as 1000 fps. The sample object was a metal rod 2.6 mm in diameter. The rod was hung by a string and, when at rest, placed vertically at the center of the THz beam at a distance of $3f$ from the TPX lens. Real-time images of the rod, while swinging, were obtained. The CCD camera captured an image for each probe pulse that mapped the THz field on the EO crystal. The THz image shows the shadow of the metal rod, as the dark area, where THz waves could not pass through.

The resulting images were contaminated by a variety of noise, particularly significant among them was at from the CCD camera. In this experiment, photon noise and thermal noise were dominant because the probe pulse was weak and the images were taken at a high frame rate. The photon noise occurred because of incorrect counting of the same number of photons for consecutive frames. In addition, thermal noise

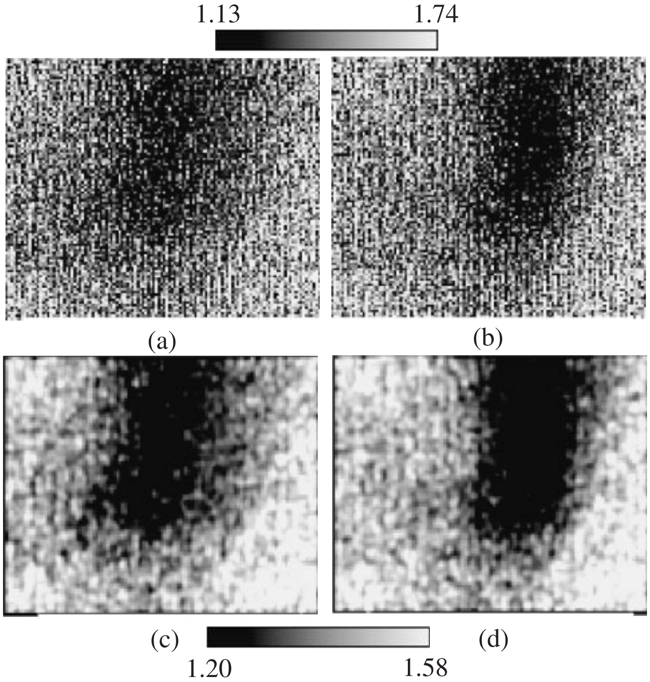

Fig. 3. Shadow of metal rod detected by single-shot THz pulse (a) and (b) obtained by dividing the sample image data (with rod) by the reference image data (without rod). Image (b) was obtained 20 ms after image (a). Images (c) and (d) are the results of applying a Gaussian filter operator to images (a) and (b), respectively. The upper and lower bars indicate the gray scale for the upper and lower images. The values of each image are mapped in the percentile range of 10%–90%. The images correspond to dimensions of $8.8 \times 7.4\,\mathrm{mm}^2$ on the object plane.

was from a stochastic source of electrons in a CCD well. Other noise came from laser instability. This noise can be reduced by image processing.

When the image quality is low, a level-detecting method cannot find the object reliably. Therefore, image processing was designed according to the following steps: (a) correct for nonuniformity in the THz beam and (b) suppress noise. The effect of the dark hole at the center of the images, which was attributed to the focusing characteristics of half-cycle THz pulses,[15] was reduced by dividing the image data by the reference field image, namely, the image of the THz field when the sample object was removed. The resultant images are shown in Figs. 3(a) and 3(b). Image (b) was obtained 20 ms after image (a). They have been cropped, into 120×100 pixels, to show the area surrounding the subject of the interest, corresponding to dimensions of $8.8 \times 7.4\,\mathrm{mm}^2$ on the object plane. This process revealed the real shape of the rod as a dark area.

The use of the Gaussian kernel for noise filtering has become popular. This has been applied in several areas such as edge finding and scale-space analysis. The Gaussian filter in spatial domain is expressed as

$$h(x, y) = \left(\frac{1}{\sqrt{2\pi}\sigma}\exp\left(-\frac{x^2}{2\sigma^2}\right)\right) \cdot \left(\frac{1}{\sqrt{2\pi}\sigma}\exp\left(-\frac{y^2}{2\sigma^2}\right)\right), \tag{2}$$

where x and y are the spatial coordinates and σ is the

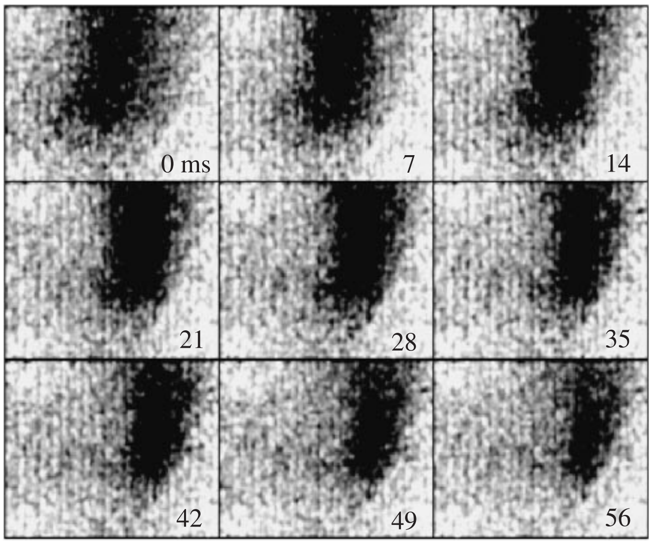

Fig. 4. Photographs of movie showing translation of metal rod from left to right with time interval of 7 ms. The plot parameters were the same as those used in Fig. 3.

variance. Since commercially available image processing software typically affects only one image at a time, we implemented a computer program that can manipulate the entire set of images at one time. This provides an efficient conceptual framework for image processing tasks. To carry out the image processing, zeros were padded to the divided images to make the data size in each dimension $N = 256$. The images were two-dimensionally Fourier transformed and multiplied by the Fourier transform of the filter function. They were then inversely transformed to spatial domain data and the padded portion cut out. The results of applying the Gaussian filter operator with a variance of 1 are shown in Figs. 3(c) and 3(d). Obviously, Gaussian filtering produced clearer images. It should be noted that a larger variance in filtering makes the image clearer but sharp edges and specular highlights may be softened. The calculation processes took 0.5 second per frame on a PC. Figure 4 shows more photographs of the Gaussian-filtered data representing the movement of the rod from left to right in 56 ms. The time interval between two adjacent images was selected to be 7 ms for observing the change. Frequency components that can resolve the object were only found in the central area of the image. The part of the rod that was out of the THz beam or in the nonactive area of the EO crystal (the right bottom corner) appeared bright. This effect can be seen in the photographs at 49 and 56 ms.

In conclusion, 1 kHz THz field imaging was demonstrated using a single THz pulse for each image. Image quality has been improved by dividing with the reference image and Gaussian filtering. The observation of high-speed events with THz radiation is realized at a temporal resolution of 1 ms for the first time. Further improvement should concentrate on increasing the spatial resolution such as the reduction in the number of low-frequency components that blurs images.

This study was partly supported by the 21st Century Center of Excellence Program "Promotion of Creative Interdisciplinary Materials Science for Novel Functions".

1) D. Grischkowsky, S. Keiding, M. van Exter and Ch. Fattinger: J. Opt. Soc. Am. B **7** (1990) 2006.
2) M. Walther, B. Fischer, M. Schall, H. Helm and P. U. Jepsen: Chem. Phys. Lett. **332** (2000) 389.
3) K. Okumura and Y. Tanimura: Chem. Phys. Lett. **295** (1998) 298.
4) E. Pickwell, B. E. Cole, A. J. Fitzgerald, M. Pepper and V. P. Wallace: Phys. Med. Biol. **49** (2004) 1595.
5) Q. Wu, T. D. Hewitt and X.-C. Zhang: Appl. Phys. Lett. **69** (1996) 1026.
6) Z. Jiang and X.-C. Zhang: Opt. Express **5** (1999) 243.
7) M. Usami, T. Iwamoto, R. Fukusawa, M. Tani, M. Watanabe and K. Sakai: Phys. Med. Biol. **47** (2002) 3749.
8) F. Miyamaru, T. Yonera, M. Tani and M. Hangyo: Jpn. J. Appl. Phys. **43** (2004) L489.
9) G. L. Eesley, M. D. Levenson and M. W. Tolles: IEEE J. Quantum Electron. **14** (1978) 45.
10) Z. Jiang, F. G. Sun, Q. Chen and X.-C. Zhang: Appl. Phys. Lett. **74** (1999) 1191.
11) T. Hattori, K. Ohta, R. Rungsawang and K. Tukamoto: J. Phys. D **37** (2004) 770.
12) R. Rungsawang, K. Tukamoto and T. Hattori: to be published in Jpn. J. Appl. Phys.
13) P. Sang-Gyu, A. M. Weiner, M. R. Melloch, C. W. Siders, J. L. W. Siders and A. J. Taylor: IEEE J. Quantum Electron. **35** (1999) 1257.
14) T. Hattori, R. Rungsawang, K. Ohta and K. Tukamoto: Jpn. J. Appl. Phys. **41** (2002) 5198.
15) R. Rungsawang, K. Ohta, K. Tukamoto and T. Hattori: J. Phys. D **36** (2003) 229.